Journal of Veterinary Cardiology (2019) **24**, 28—35

Journal of Veterinary Cardiology
ESVC

www.elsevier.com/locate/jvc

Case Report

Anatomical assessment of intrathoracic cardiovascular structures using fast spin-echo double inversion recovery and steady-state free precession magnetic resonance imaging in a normal cat

A. Arencibia, DVM, PhD[a,*], J.A. Corbera, DVM, PhD[b], F. Gil, DVM, PhD[c], G. Ramírez, DVM, PhD[c], J.R. Jaber, DVM, PhD[a], M. Morales, DVM, PhD[b], J.M. Vázquez, DVM, PhD[c]

[a] *Department of Morphology, Veterinary Faculty, University of Las Palmas de Gran Canaria, 35413, Arucas (Las Palmas), Spain*
[b] *Department of Animal Pathology, Veterinary Faculty, University of Las Palmas de Gran Canaria, 35413, Arucas (Las Palmas), Spain*
[c] *Department of Veterinary Anatomy and Pathological Anatomy, Veterinary Faculty, University of Murcia, 30100, Murcia, Spain*

Received 22 November 2018; received in revised form 6 May 2019; accepted 7 May 2019

KEYWORDS
Dark-blood imaging;
Bright-blood imaging;
structures;
Feline

Abstract In human medicine, non-contrast cardiac magnetic resonance imaging (CMRI) is routinely used to assess the cardiovascular system. In this study, using non-contrast CMRI, we provide a thorough description of the normal appearance of the intrathoracic cardiovascular structures in one healthy cat using a magnet operating at a field of 1.5-Tesla. The CMRI protocol was based on the use of fast spin-echo double inversion recovery and steady-state free precession pulse sequences in oblique short-axis, vertical long-axis, and horizontal long-axis imaging planes. After imaging the feline heart, four cadaver cats injected with latex substance into their arterial and venous systems were sectioned to facilitate interpretation of the intrathoracic cardiovascular structures to the corresponding CMRI. The fast spin-echo double inversion recovery images showed the best evaluation of gross intrathoracic anatomy, giving excellent contrast of the myocardium and vessels walls as they appeared with intermediate signal intensity compared to the lumen that

* Corresponding author.
E-mail address: alberto.arencibia@ulpgc.es (A. Arencibia).

https://doi.org/10.1016/j.jvc.2019.05.002

appeared with low signal intensity. By contrast, steady-state free precession images showed details of the heart cavities and vascular lumen due to the high signal intensity of fast-flowing blood. The results of this study provide some anatomic detail for the heart and associated vessels as seen by non-contrast CMRI in the domestic cat.

Non-contrast magnetic resonance angiography is a non-invasive group of imaging techniques based on magnetic resonance imaging for the anatomical and functional assessment of intrathoracic cardiovascular structures. These techniques include black-blood and bright-blood imaging [1—3]. Black-blood fast spin-echo inversion recovery sequences are acquired to null the signal from flowing blood or fat in the resulting image. The inversion recovery technique uses a selective and a non-selective 180° inversion pulse followed by a long inversion time to null blood magnetization. A second selective 180° inversion pulse can also be applied to null the signal from fat in the resulting image. This is referred to as double or triple inversion recovery. These sequences are useful for visualizing the walls of the cardiac chambers and blood vessels. By contrast, bright-blood steady-state free precession (SSFP) sequences are based on fast gradient-echo acquisitions in which both components of magnetization (transverse and longitudinal) are kept in constant magnetization through the use of a repetition time that is shorter than the T2 relaxation time of tissue. The SSFP sequence describes the high signal intensity of fast-flowing blood and is used for evaluating cardiac morphology and function [1—3].

A 3-year-old, 3 kg, male, domestic cat was used for this cardiac magnetic resonance imaging (CMRI) study. Written informed consent was obtained from the owner of the cat used for this research. This CMRI anatomical study was approved by the Ethical Commission of Veterinary Medicine of Las Palmas de Gran Canaria University (protocol number: MV-2015/08). The cat was premedicated with butorphanol[d] (0.1 mg/kg), dexmedetomidine[e] (0.075 mg/kg), and ketamine[f] (15 mg/kg) intramuscularly. After premedication, a heparinized intravenous catheter and physiologic saline at 5 mL/h were placed in the cephalic vein. Anesthesia was induced with propofol[g] (10 mg/kg intravenous). A vaporizer[h] with sevoflurane[i] (2—3%) in an O_2 flow of 0.8 l/min was used for anesthetic maintenance. Mechanical ventilation[j] was used throughout the study.

Non-contrast CMRI was acquired using a magnet operating at a field of 1.5-Tesla[k], and a human thorax coil of 8-channel was used. For timing of data acquisition, the animal was placed in dorsal recumbency, and retrospective electrocardiographic gating was used to mitigate the heart motion and pulsatility of the great vessels. No respiratory gating was used; the cat was mechanically ventilated at rate of 10—12 breaths/min. The images were acquired with hyperventilation-induced apnea. In this study, fast spin-echo double inversion recovery (FSE-DIR) and SSFP pulse sequences were used to generate short-axis, vertical long-axis, and horizontal long-axis planes. The cardiac planes were established on standard protocols described for humans. The short axis was extended perpendicular to the longitudinal axis of the heart at the level of the mid left ventricle, and images were performed in a craniocaudal direction from the cranial vena cava and brachiocephalic trunk (BT) to the apex of the heart. The vertical long axis was generated along a vertical plane to the short-axis plane, and the images were

Abbreviations

BT	brachiocephalic trunk
CMRI	cardiac magnetic resonance imaging
DAo	descending aorta
FSE-DIR	fast spin-echo double inversion recovery
SSFP	steady-state free precession
TE	echo time
TR	repetition time

[d] Torbugesic; Zoetis, SLU, Madrid, Spain.
[e] Dexdormitor; Lab. Dr. Esteve SAU, Barcelona, Spain.
[f] Imalgene; Merial Laboratorios, Barcelona, Spain.
[g] Propovet; Lab. Dr. Esteve SAU, Barcelona, Spain.
[h] Sigma Delta Vaporizer Penlon, Dräguer plug-in; PenlonLimited, Abingdon, UK.
[i] Sevoflo; Abbot Laboratories SA, Madrid, Spain.
[j] Ventilator V725000 SurgiVet; Smith Medical PM, Inc, Norwell, MA.
[k] Signa Excite; General Electric Medical Systems, Madrid, Spain.

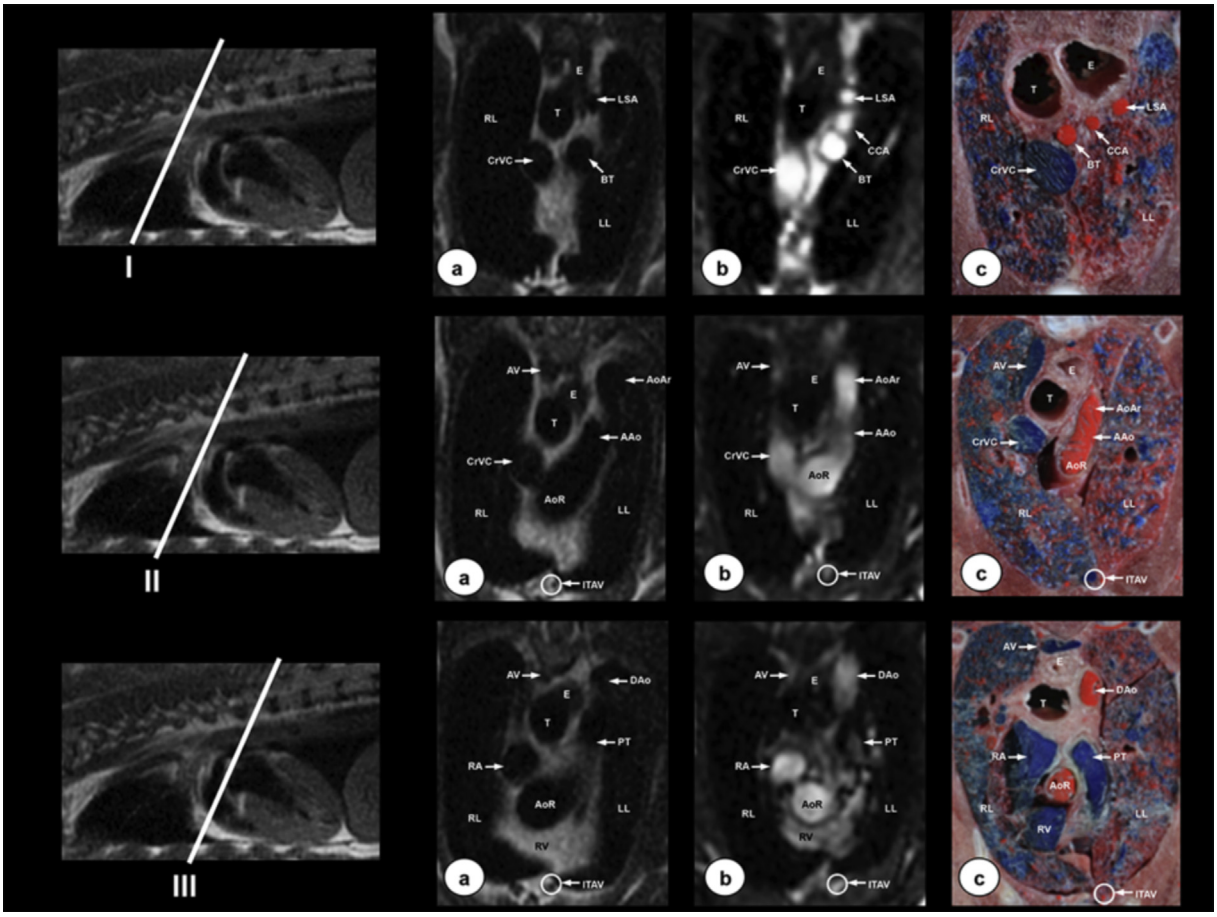

Fig. 1 Short-axis images at the level of the cranial vena cava and brachiocephalic trunk (level I), ascending aorta (level II), and pulmonary trunk (level III): (a) FSE-DIR CMRI, (b) SSFP CMRI, and (c) anatomical section. Images are oriented so that the right side of the heart is to the right and the dorsal surface is at the top. AAo, ascending aorta; AoAr, aortic arch; AoR, aortic root; AV, azygos vein; CCA, common carotid artery; BT, brachiocephalic trunk; CrVC, cranial vena cava; DAo, descending aorta; E, esophagus; ITAV, internal thoracic artery and vein; LL, left lung; LSA, left subclavian artery; PT, pulmonary trunk; RA, right atrium; RL, right lung; RV, right ventricle; T, trachea; CMRI, cardiac magnetic resonance imaging; FSE-DIR, fast spin-echo double inversion recovery; SSFP, steadystate free precession.

obtained in a direction from the auricular face to atrial face of the heart. The horizontal long axis was established selecting the horizontal plane that is perpendicular to the short axis, and the images were performed in a dorsoventral direction from the descending aorta (DAo) to the apex of the heart. The FSE-DIR short-axis images were obtained using the following parameters: echo time (TE), 43.5 ms; repetition time (TR), 1348 ms; 3-mm slice thickness with 3.5-mm spacing between slices and a matrix of 224 × 224. Acquisition time was 26 s. For SSFP short-axis images, the TE was 1.8 ms, TR was 5.3 ms, and there was 3-mm slice thickness with 3.5-mm interslice spacing and a matrix of 224 × 224. Acquisition time was 30 s. For FSE-DIR vertical long-axis images, the TE was 41.1 ms, TR was 1538.4 ms, and there was 3-mm slice thickness with 3.5-mm interslice spacing and a matrix of 224 × 224. Acquisition time was 26 s. For SSFP vertical long-axis images, the TE was 2.1 ms, TR was 7.7 ms, there was 4-mm slice thickness with 4.5-mm interslice spacing, and the matrix was 224 × 224. Acquisition time was 48 s. For FSE-DIR horizontal long-axis images, the TE was 39.4 ms, TR was 1348.3 ms, there was 4-mm slice thickness with 3.5-mm interslice spacing, and the matrix was 224 × 224. Acquisition time was 26 s. For SSFP horizontal long-axis images, the TE was 1.9 ms, TR was 5.7 ms, there was 4-mm slice thickness with 4-mm interslice spacing, and the matrix was 224 × 224. Acquisition time was 26 s.

In addition, gross sections of the thorax from cadaver cats were used to facilitate a better interpretation of the CMRI. Therefore, four cross-breed cadaver cats belonging to the Zoonosis Service of Murcia (Spain) were used. Animals were humanely euthanized for reasons unrelated to this

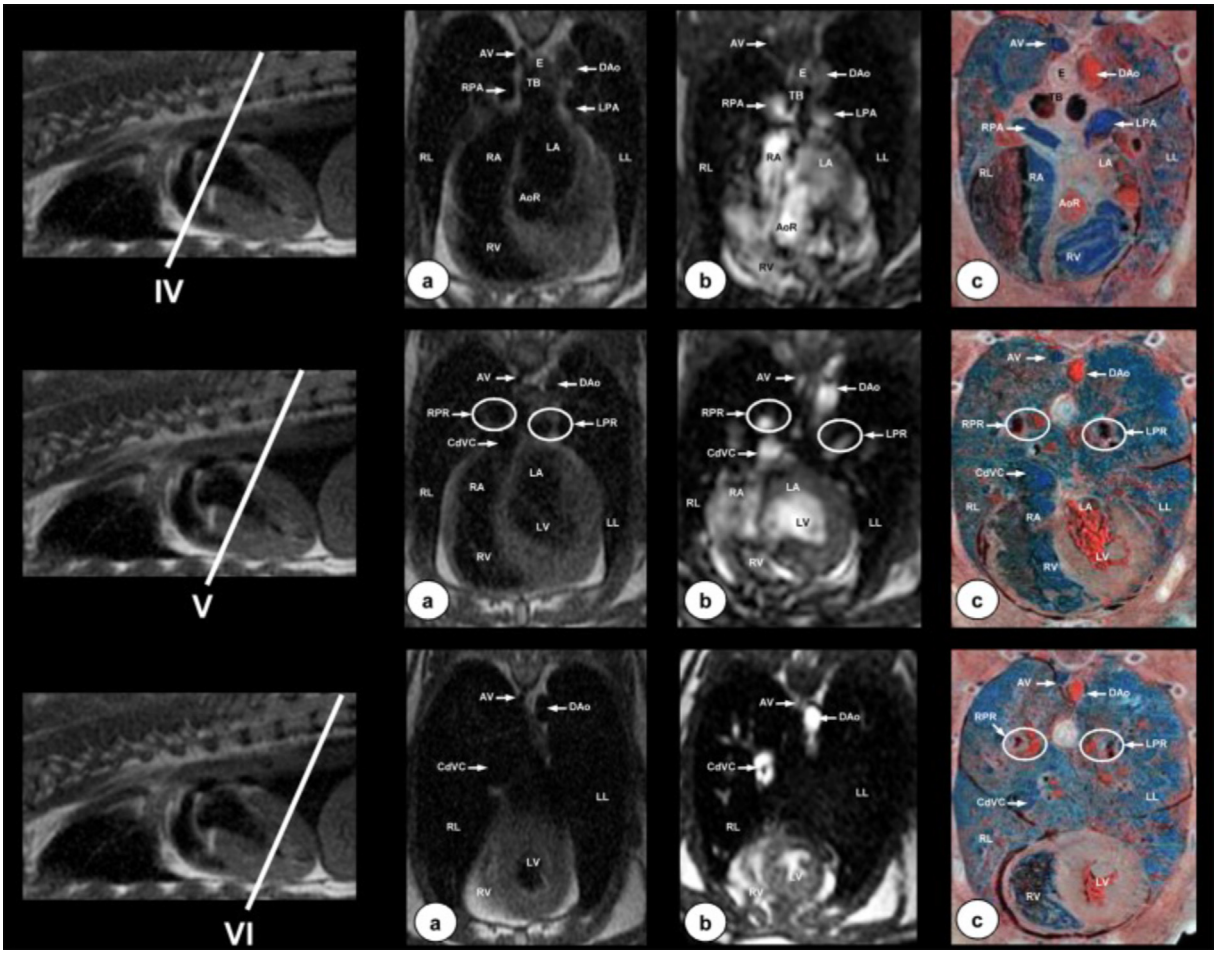

Fig. 2 Short-axis images at the level of the pulmonary arteries (level IV), caudal vena cava ending into the right atrium (level V), and left ventricle (level VI): (a) FSE-DIR CMRI, (b) SSFP CMRI, and (c) anatomical section. Images are oriented so that the right side of the heart is to the right and the dorsal surface is at the top. AoR, aortic root; AV, azygos vein; CdVC, caudal vena cava; DAo, descending aorta, E, esophagus; LA, left atrium; LL, left lung; LPA, left pulmonary artery; LPR, left pulmonary root, LV, left ventricle; RA, right atrium; RL, right lung; RPA, right pulmonary artery; RPR, right pulmonary root; RV, right ventricle; TB, tracheal bifurcation; CMRI, cardiac magnetic resonance imaging; FSE-DIR, fast spin-echo double inversion recovery; SSFP, steadystate free precession.

study. The cadaver cats were bled-out with saline solution, and latex was injected: red latex filled systemic arteries and pulmonary veins, whereas the blue latex filled systemic veins and pulmonary arteries. The injected cats were then frozen at −70 °C for 7 days and sliced into contiguous 1.5-cm-thick sections to assist in the interpretation of anatomical structures.

Intrathoracic cardiovascular structures were evaluated according to their characteristic signal intensity (dark- or bright-blood images) and compared with the corresponding gross sections (Figs. 1—4). The short-axis images are shown in Figs. 1 and 2. These figures are shown from the cranial vena cava and BT (level I) to the left ventricle (level VI). Fig. 3 corresponds to the vertical long axis at level of the BT (level I) and the aortic arch and DAo (level II). The horizontal long-axis images are shown in Fig. 4 at level of the pulmonary trunk and ascending aorta.

In this study, FSE-DIR pulse sequence showed the fast-flowing blood with low signal intensity (dark-blood images) compared with the SSFP pulse sequence, where blood appeared with high signal intensity (bright-blood images). Thus, the aortic root and the ascending aorta beginning in the left ventricle were identified in the short-axis images corresponding to Fig. 1 (level II) and in the vertical long-axis (Fig. 3) and horizontal long-axis (Fig. 4) image planes. The main branches of the aorta such as the BT, the left subclavian artery, and the DAo were also visible. The BT, which is to the right and slightly cranial to the other two branches, could be identified in Fig. 1 (level I) and

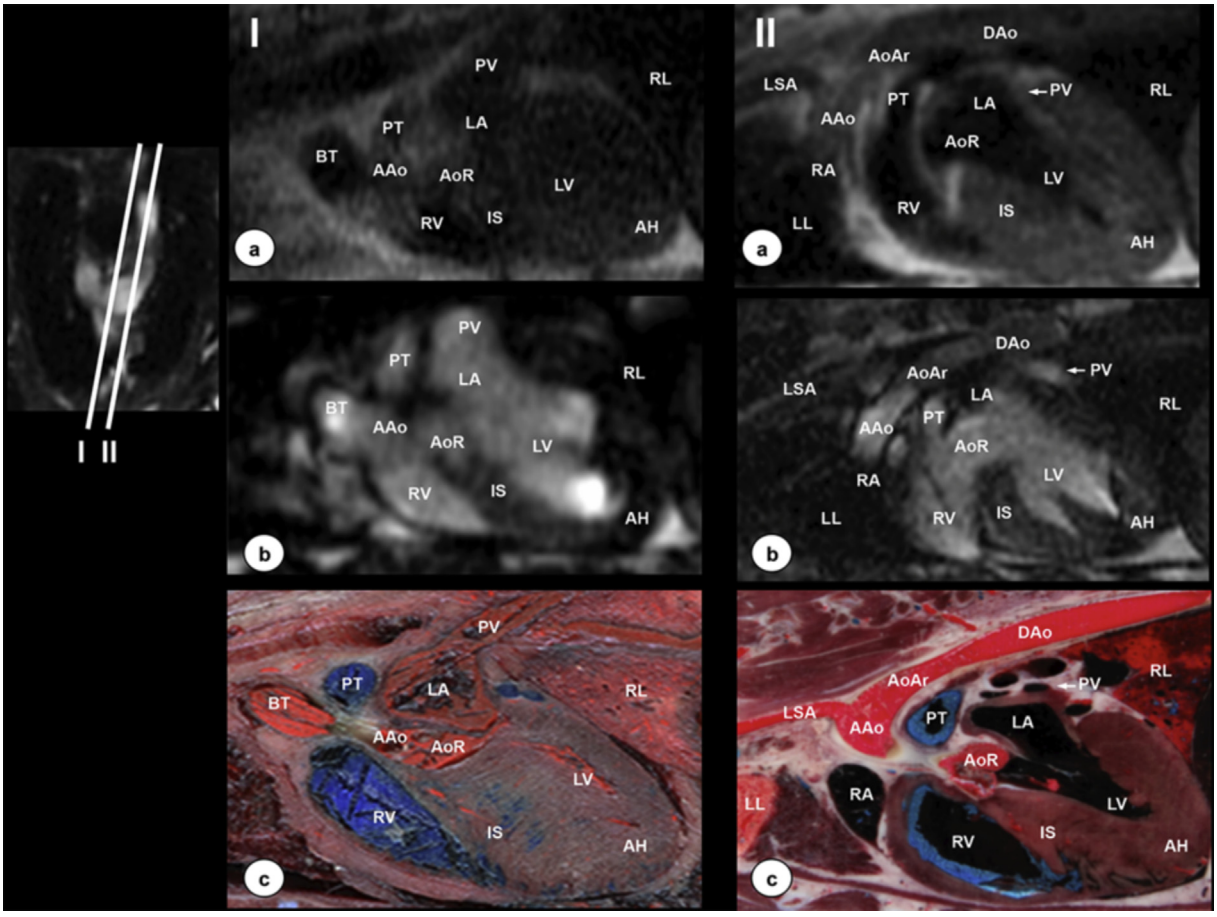

Fig. 3 Vertical long-axis images at the level of the brachiocephalic trunk (level I) and aortic arch and descending aorta (level II): (a) FSE-DIR CMRI, (b) SSFP CMRI, and (c) anatomical section. Images are oriented so that the left is cranial and the right is caudal. AAo, ascending aorta; AH, apex of the heart; AoAr, aortic arch; AoR, aortic root; BT, brachiocephalic trunk; DAo, descending aorta; IS, interventricular septum; LA, left atrium; LL, left lung; LV, left ventricle; LSA, left subclavian artery; PT, pulmonary trunk; PV, pulmonary vein; RA, right atrium; RL, right lung; RV, right ventricle; CMRI, cardiac magnetic resonance imaging; FSE-DIR, fast spin-echo double inversion recovery; SSFP, steadystate free precession.

3 (level I). The left subclavian artery, which is to the left of the BT, was visible in the short-axis images corresponding to Fig. 1 (level I) and vertical long-axis images corresponding to Fig. 3 (level II). The aortic arch between the ascending aorta and the DAo was especially seen in the vertical long-axis images (Fig. 3, level II), whereas the course of the DAo arising from the aortic arch was easily identified in the short-axis images corresponding to Fig. 1 (level III) and Fig. 2 (levels IV—VI) and in the vertical long-axis images corresponding to Fig. 3 (level II). Furthermore, the pulmonary trunk arising from the right ventricle was clearly visible in the short-axis plane (Fig. 2, level IV), as well in the vertical (Fig. 3, levels I and II) and horizontal (Fig. 4) long-axis images. The cranial vena cava and caudal vena cava were observed entering into the right atrium, especially in Fig. 1 (levels I—III) and Fig. 2 (levels V and VI). The course of the azygos vein to the right side of the vertebral column was identified in the Fig. 1 (level II and III) and 2 (levels IV—VI). Other main vessels such as pulmonary arteries and veins were better identified in the SSFP images than in FSE-DIR images especially in Fig. 2 (levels IV and V) and in the vertical long-axis plane images corresponding to Fig. 3. In addition, the branches of pulmonary arteries and veins at the level of the pulmonary roots were only defined in the transverse images corresponding to Fig. 2 (levels V and VI), whereas the internal thoracic arteries and veins were especially shown in Fig. 1 (levels II and III). In all images, the cardiac walls showed intermediate signal intensity, but they were best observed in the FSE-DIR images compared with SSFP images.

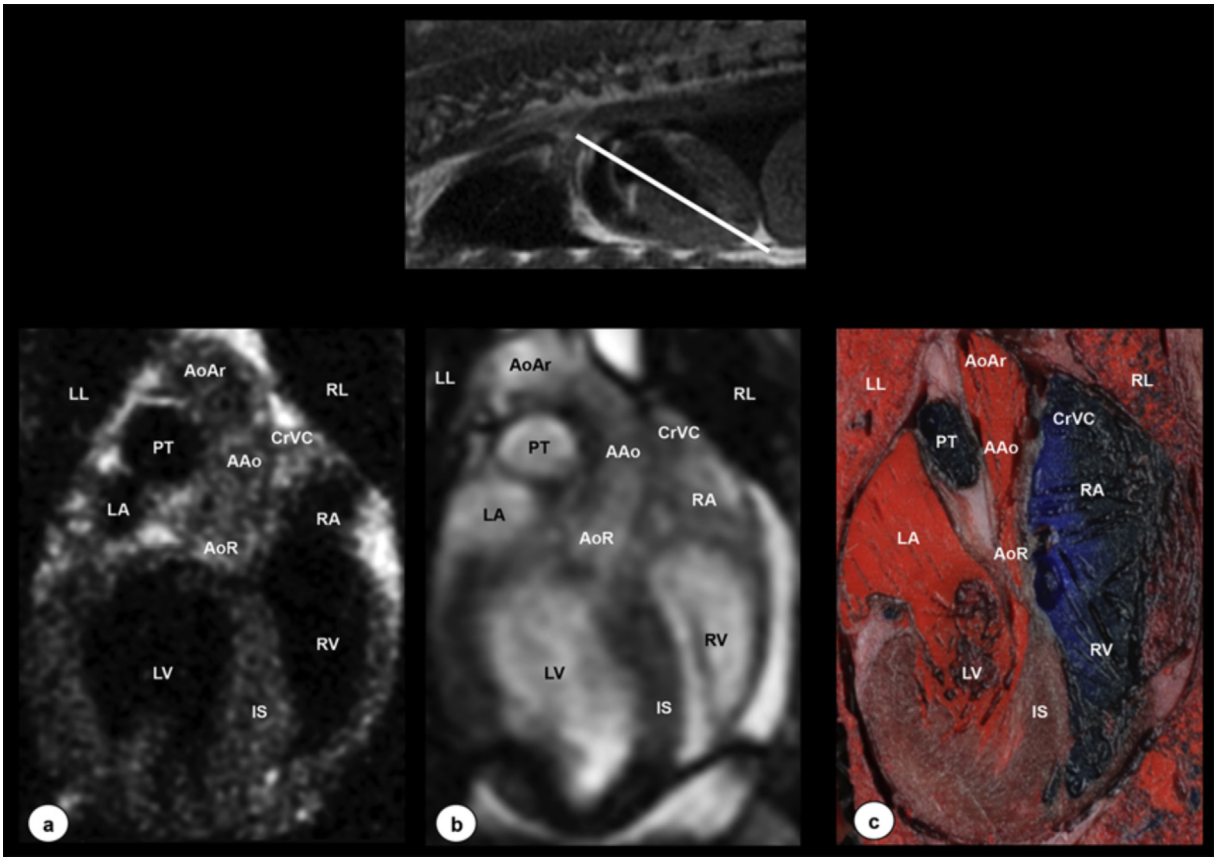

Fig. 4 Horizontal long-axis images at the level of the pulmonary trunk and ascending aorta: (a) FSE-DIR CMRI, (b) SSFP CMRI, and (c) anatomical section. Images are oriented so that the right side of the heart is to the right and the top is cranial. AAo, ascending aorta; AoAR: aortic arch; AoR, aortic root; CrVC, cranial vena cava; IS, interventricular septum; LA, left atrium; LL, left lung; LV, left ventricle; PT, pulmonary trunk; RA, right atrium; RL, right lung; RV, right ventricle; CMRI, cardiac magnetic resonance imaging; FSE-DIR, fast spin-echo double inversion recovery; SSFP, steadystate free precession.

Discussion

In human cardiology, advances in CMRI pulse sequences have made it possible to perform studies of the heart and great vessels. So, CMRI has become the modality of choice for morphological and functional assessment, as well as for the diagnosis and management of diseases of the cardiovascular system [1—3]. In veterinary medicine, several CMRI studies have primarily been reported in basic and clinical research in dogs [4—7] and cats [8—11]. The advantages of non-contrast enhanced CMRI compared with echocardiography include high spatial resolution images of the heart and the ability to acquire images in every potential spatial plane without being limited by acoustic windows [12]. Cardiac computed tomography uses X-rays, so patient radiation constitutes the basic limitation for its use. It provides high spatial resolution and good differentiation of the lumen of the myocardium, and it is particularly useful for evaluating small and tortuous coronary arteries. By contrast, CMRI uses magnetic fields and radio frequency pulses. It has high temporal and contrast resolution, which enables high accuracy in evaluating ventricular function, being the gold standard. Hence, CMRI allows better differentiation between the myocardium and blood and tissue characteristics (e.g., fibrosis, fat infiltration) that cannot be detected by cardiac computed tomography. Besides, CMRI allows evaluation of anatomy and function, flow quantification, and viability studies of the myocardium [2,12].

In veterinary medicine, the major disadvantages of CMRI include cost, limited equipment availability, long scan times, the need for general anesthesia, and lack of experience in obtaining and analyzing CMRI [5,8]. Other significant drawbacks include the rapid and complex movements of the heart, vascular pulsatility and respiratory motion. Interestingly, during the first sequences of this study, movement artifacts were detected due to the heart motion. Later, a more stable anesthesia was completed, and a reduction

of the heart rate from an average rate of 130—150 bpm to an average rate of 90—110 bpm was measured. Probably, this lower heart rate provided us better imaging acquisition without movement artifacts. The use of cardiac and respiratory gating as well as rapid and high-performance gradients and advanced CMRI pulse sequences help to minimize the imaging artifacts improving the image resolution [1,5,8].

Interpretation of CMRI studies requires an understanding of the basic pulse sequences, cardiac anatomy, and standard imaging planes [1]. In humans, numerous pulse sequences or software programs have been applied to CMRI. Traditionally, spin-echo and gradient-echo sequences have been used for dark-blood imaging or bright-blood imaging, respectively. However, these techniques have been supplanted by the newer fast spin-echo and gradient-echo pulse sequences, which allow rapid imaging that minimizes the effects of cardiac and respiratory motion [1—3]. These pulse sequences provide anatomical and functional information with greater ability to distinguish between vascular and non-vascular structures. In this study, FSE-DIR and SSFP pulse sequences were selected to obtain dark-blood and bright-blood angiography images. The FSE-DIR pulse sequence for dark-blood images is commonly used to further null the signal from blood for black-blood imaging, thereby improving contrast between the cardiac tissues and the blood pool [1,3]. The FSE-DIR sequence provided an overview of gross intrathoracic anatomy and better cardiac wall border definition compared with SSFP. However, the FSE-DIR sequence did not allow us to distinguish between blood vessels and bronchi compared with SSFP. By contrast, the SSFP sequence shows the appearance of the blood with high signal intensity compared with the myocardium [1—3]. Similar advance pulse sequences have been reported in CMRI studies in dogs [4—7] and cats [8—11].

In this study, CMRI planes provided adequate information of midline thoracic vascular structures (vertical long-axis plane), good depiction of the chambers of the heart (short-axis plane), as well as offered standard references for the size and positions of the heart and major blood vessels (horizontal long-axis plane). Similar CMRI planes have been used in other studies performed in humans [1—3], dogs [4—7], and cats [8—11]. Nonetheless, in most of these studies, vascular structures were only described in short-axis and/or horizontal long-axis planes, and morphologic assessment of midline thoracic vascular structures was limited due to the absence of vertical long-axis planes. In addition, the gross sections performed with colored latex substance in this study were a helpful tool for the better identification of the cardiac and vascular structures in the images presented by CMRI.

In humans, advanced CMRI pulse sequences now are available for evaluating a wide variety of congenital and acquired heart diseases [1,2]. With improvements in CMRI protocols and optimized gradient systems, magnetic resonance angiography images are a promising, non-invasive, and accurate method for evaluating the feline heart and associated vessels [8—11]. Therefore, an accurate anatomical interpretation of these images would be useful for the assessment of intrathoracic anatomical structures such as vessels, lungs, bronchia, or esophagus and could be used in the diagnosis of several heart diseases described in feline medicine such as cardiac masses [13] and congenital anomalies [14]. In the present study, FSE-DIR and SSFP pulse sequences used to obtain dark-blood and bright-blood images provided some valuable anatomical information of the feline heart and argue for further use and development of CMRI in feline medicine.

Conflict of Interest Statement

The authors do not have any conflicts of interest to disclose.

Acknowledgments

CMRI acquisitions were financed with funding from the Department of Morphology of Las Palmas de Gran Canaria University (Spain). Gross anatomical dissections were financed with funding from the Department of Veterinary Anatomy and Pathological Anatomy of Murcia University (Spain).

References

[1] Ginat DT, Fong MW, Tuttle DJ, Hobbs SK, Vyas RC. Cardiac imaging: Part 1, MR pulse sequences, imaging planes, and basic anatomy. AJR Am J Roentgenol 2011;197:808—15.
[2] Earls JP, Ho VB, Foo TK, Castillo E, Flamm SD. Cardiac MRI: recent progress and continued challenges. J Magn Reson Imaging 2002;16:111—27.
[3] Kastler B. Cardiovascular anatomy and atlas of MR normal anatomy. In: Kastler, editor. MRI of Cardiovascular Malformations. Berlin: Springer; 2011. p. 17—39.
[4] Gilbert SH, McConnell FJ, Holden AV, Sivananthan MU, Dukes-McEwan J. The potential role of MRI in veterinary clinical cardiology. Vet J 2010;183:124—34.
[5] Contreras S, Arencibia A, Gil F, De Miguel A, Ramírez G, Vázquez JM. Black and bright-blood sequences magnetic resonance angiography and gross sections of the canine thorax: an anatomical study. Vet J 2010;185:231—4.

[6] Sieslack AK, Dziallas P, Nolte I, Wefstaedt P, Hungerbühler SO. Quantification of right ventricular volume in dogs: a comparative study between three-dimensional echocardiography and computed tomography with the reference method magnetic resonance imaging. BMC Vet Res 2014;10:242.
[7] Eskofier J, Wefstaedt P, Beyerbach M, Nolte I, Hungerbühler SO. Quantification of left ventricular volumes and function in anesthetized beagles using real-time three-dimensional echocardiography: 4D-TomTec™ analysis versus 4D-AutLVQ™ analysis in comparison with cardiac magnetic resonance imaging. BMC Vet Res 2015;11:260.
[8] MacDonald KA, Kittleson MD, Reed T, Larson R, Kass P, Wisner ER. Quantification of left ventricular mass using cardiac magnetic resonance imaging compared with echocardiography in domestic cats. Vet Radiol Ultrasound 2005;46:192—9.
[9] MacDonald KA, Kittleson MD, Larson RF, Kass P, Klose T, Wisner ER. The effect of ramipril on left ventricular mass, myocardial fibrosis, diastolic function, and plasma neurohormones in Maine coon cats with familial hypertrophic cardiomyopathy without heart failure. J Vet Intern Med 2006;20:1093—105.
[10] MacDonald KA, Wisner ER, Larson RF, Klose T, Kass PH, Kittleson MD. Comparison of myocardial contrast enhancement via cardiac magnetic resonance imaging in healthy cats and cats with hypertrophic cardiomyopathy. Am J Vet Res 2005;66:1891—4.
[11] MacDonald KA, Kittleson MD, Garcia-Nolen T, Larson RF, Wisner ER. Tissue Doppler imaging and gradient echo cardiac magnetic resonance imaging in normal cats and cats with hypertrophic cardiomyopathy. J Vet Intern Med 2006;20:627—34.
[12] Shah S, Chryssos ED, Parker H. Magnetic resonance imaging: a wealth of cardiovascular information. Ochsner J 2009;9:266—77.
[13] Treggiari E, Pedro B, Dukes-McEwan J, Gelzer AR, Blackwood L. A descriptive review of cardiac tumours in dogs and cats. Vet Comp Oncol 2017;15:273—88.
[14] Scansen BA, Schneider M, Bonagura JD. Sequential segmental classification of feline congenital heart disease. J Vet Cardiol 2015;17:S10—52.